Polyether, Poly(*N*,*N*-dimethylacrylamide), and $LiClO_4$ Composite Polymeric Electrolytes

W. Wieczorek, A. Zalewska,† D. Raducha, Z. Florjańczyk,† and J. R. Stevens*

Department of Physics, University of Guelph, N1G 2W1 Guelph, Ontario, Canada

A. Ferry and P. Jacobsson

Department of Experimental Physics, Umeä University, S-90187 Umeä, Sweden

Received May 16, 1995; Revised Manuscript Received August 10, 1995[⊗]

ABSTRACT: The results of detailed studies of the ionic conductivity, ultrastructure, and morpholgy of polyether−poly(*N*,*N*-dimethylacrylamide)−$LiClO_4$ electrolytes are presented and discussed. These composite electrolytes have been studied using differential scanning calorimetry (−110−150 °C), with FT-IR spectroscopy (20−85 °C) and impedance analysis (−20−100 °C). Room temperature FT-Raman spectroscopy, SEM, and X-ray energy dispersive studies have also been performed. Highly crystalline poly(ethylene oxide) and amorphous or low-crystalline oxymethylene-linked poly(ethylene oxide) are used as polyether matrices for composite electrolytes. It is shown that interactions of lithium cations with polyether oxygens and the carbonyl oxygens of the "filler" poly(*N*,*N*-dimethylacrylamide) lead to the formation of various types of complexes. These interactions can be classified as Lewis acid−base reactions. The formation of different types of complexes modifies the ultrastructure and enhances the subambient and ambient temperature ionic conductivity of these electrolytes in comparison to the pure polyether−$LiClO_4$ electrolyte. The increase in the conductivity is attributed to the presence of a highly flexible uncomplexed polyether phase surrounding filler particles. The temperature dependence of ionic conductivity is Arrhenius at ambient and subambient temperatures and VTF at higher temperatures. The order−disorder transition temperature calculated on the basis of a semiempirical model is found to be equal to the onset temperature of the melting peak of the crystalline poly(ethylene oxide) for these semicrystalline electrolytes or equal to 1.2 times the glass transition temperature of the polyether−$LiClO_4$ electrolyte for the corresponding amorphous systems. Assuming that the enhanced conductivity of these composite polymer electrolytes is associated with interphase phenomena, the conductivity results were analyzed in terms of a model based on effective medium theory.

Introduction

Polymer solid electrolytes based on polyether matrices have recently attracted considerable attention[1−3] due mainly to the possibility of their application in various electrochemical devices such as alkali metal batteries, electrochromic displays and sensors, and fuel cells working at ambient and moderate temperatures. It has been found that the polymer and ion motions are coupled,[4] and hence the presence of a flexible, amorphous polyether phase is essential for high ionic conductivity in polymeric electrolytes.[5] Several attempts have been made to obtain amorphous polyether matrices which exhibit good mechanical properties and stability over a wide temperature range.[2−3] The utilization of polymer blends and composites in which high molecular weight polymers or inorganic (ceramic) powders are added to the polyether−alkali metal salt complex seems to be the easiest way to achieve these polyether conductors.[2] It has been demonstrated that the addition of finely divided inorganic filler powders leads to an increase in the conductivity of polyether-based electrolytes.[6−8] This increase was suggested to be due to a decrease in the degree of crystallinity of the poly(ethylene oxide) (PEO) phase in these electrolytes which are semicrystalline at ambient temperatures.[7−8] Unfortunately the addition of ceramic particles stiffens the polyether host thus limiting the increase in conductivity.[8]

Substantial increase in the electrolyte conductivity can be obtained by the addition of polyacrylamide (PAAM).[9,10] Results from DSC studies, FT-IR spectroscopy, and EDX spectroscopy indicate that the increase in conductivity is due to enhanced segmental flexibility at the interface of the filler with the polymer matrix in the presence of alkali metal salts. This is due to the formation of complexes involving the filler and salt which results in a reduction of the number of transient cross-links between polyether oxygens and alkali metal cations. The addition of PAAM to the semicrystalline PEO-based electrolytes results in a decrease in crystallinity which also enhances the ionic conductivity.

We have proposed[11] that polymer−ion coordination phenomena occurring in these composite systems are governed by equilibria between the various Lewis acid−base reactions occurring between Lewis base centers of the polyether host, Lewis base centers on the PAAM chain, and alkali metal cations which can be treated as Lewis acids. The interpretation of these phenomena in the polyether−PAAM−alkali metal salt systems is however complicated by the possibility of the formation of hydrogen bonds between protons of NH_2 amide groups and oxyanions (such as ClO_4^-) or polyether oxygens. The competition between Lewis acid−base complex formation and hydrogen bonding leads in some cases to the lowering of the electrolyte conductivity.[10] In order to eliminate the possibility of hydrogen bonding, the organic filler was changed from PAAM to poly(*N*,*N*-dimethylacrylamide) (NNPAAM)[12] because NNPAAM lacks an amidic hydrogen. The reason for using polyacrylamides comes from the high donicity of the Lewis base centers (carbonyl oxygens and amide nitrogens) of

† On leave from the Department of Chemistry, Warsaw University of Technology, ul. Noakowskiego 3, 00-664 Warszawa, Poland.

⊗ Abstract published in *Advance ACS Abstracts,* December 1, 1995.

0024-9297/96/2229-0143$12.00/0

the polyacrylamides which for low molecular weight analogues is comparable to or even slightly higher than that of low molecular weight polyether analogues.[13−14] Preliminary results[12] show that there are strong interactions between NNPAAM and $LiClO_4$ leading to changes in the ultrastructure and conductivity of oxymethylene-linked PEO (OMPEO)−NNPAAM−$LiClO_4$ electrolytes.

In this report comprehensive studies of conductivity, phase structure, and morphology of PEO−NNPAAM−$LiClO_4$ and OMPEO−NNPAAM−$LiClO_4$ electrolytes are described. The results obtained for highly crystalline PEO-based systems are compared with those obtained for amorphous or low-crystalline OMPEO-based electrolytes. The changes in the structure and morphology are studied by the FT-IR, FT-Raman, and energy dispersive X-ray (EDX) spectroscopies and SEM techniques. These results are correlated with conductivity studies performed using impedance spectroscopy and DSC evidence for phase transitions in these composite polymeric electrolytes. The observed changes are discussed in view of Lewis acid−base type interactions occurring in the composite systems studied. It has also been shown previously[9,10] that the conductivity of the composite polymeric electrolytes can be modeled using effective medium theory (EMT) approaches. In the present paper an EMT approach which models the conductivity of polyether−NNPAAM−$LiClO_4$ composite electrolytes will be presented and discussed.

Experimental Section

Sample Preparation. NNPAAM ($M_w = 1.3 \times 10^5$; Polysciences, reagent grade) and PEO ($M_w = 5 \times 10^6$; Aldrich, reagent grade) were used without further purification after drying under vacuum at 50−70 °C for 48 h. The synthesis of OMPEO followed that of Nicholas et al.[15] The resulting transparent elastomers were dried under vacuum for 48 h before synthesizing the polymer electrolyte. Acetonitrile (Aldrich, reagent grade) was distilled twice and stored over type 4 Å molecular sieves. All of the steps in the preparation procedure were performed in an argon-filled drybox (moisture content lower than 20 ppm). $LiClO_4$ (Aldrich, reagent grade) was dried under vacuum at 120 °C prior to incorporation. The concentration of $LiClO_4$ was equal to 10 mol % with respect to the ether oxygen concentration. The solid components were mixed in appropriate amounts in a small glass reactor and then acetonitrile was added to form an ca. 5 mass % suspension with respect to all solid components. The mixture was magnetically stirred until an homogenous suspension was obtained. Excess acetonitrile was removed by vacuum distillation. The composite electrolytes obtained were dried under vacuum for 48−72 h at 60 °C. The concentration of NNPAAM in the composite electrolytes varied between 5 and 50 vol %. All samples were equilibrated at ambient temperature for at least 1 month before undertaking any experiments. EDX studies (performed for all synthesized composite polymeric electrolytes) indicated through Cl or N that both ClO_4^- and NNPAAM are homogenously distributed in these composite electrolytes.

DSC Studies. DSC data were obtained between −110 and 150°C using a DuPont TA 2910 scanning calorimeter with a low-temperature measuring head and liquid nitrogen-cooled heating element. In run 1, 15 mg samples in aluminum pans were stabilized by slow cooling to −110 °C and then heated at 10 °C/min to 150 °C. Run 2 was performed after annealing the same samples used in run 1 at 150 °C (for ca. 10−15 min) and then following the same procedure as for run 1.

Conductivity Measurements. Ionic conductivity was determined using the complex impedance method in the temperature range −20−100 °C. The samples were sandwiched between stainless steel blocking electrodes and placed in a temperature-controlled furnace. The impedance measurements were carried out on a computer-interfaced HP 4192 impedance analyzer over the frequency range 5 Hz−13 MHz. The peak to peak voltage in impedance experiments was equal to 1 V.

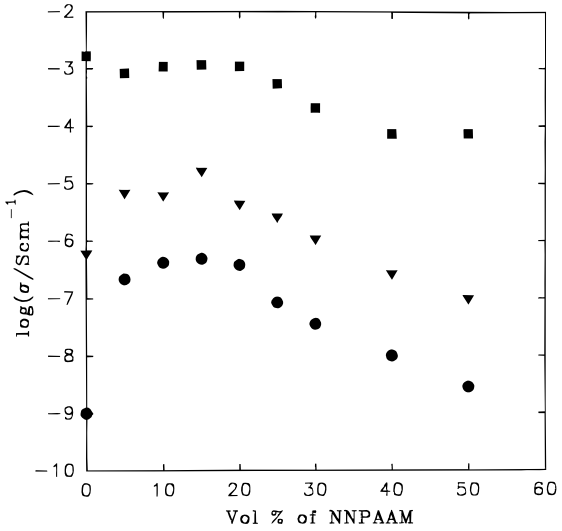

Figure 1. Isotherms of ionic conductivity of PEO−NNPAAM−$LiClO_4$ versus volume fraction of NNPAAM with 10 mol % $LiClO_4$: (●) 0 °C, (▼) 25 °C, (■) 100 °C.

FT-IR Spectroscopy. Infrared absorption spectra were recorded on a computer-interfaced Nicolet FT-IR system 4.4 instrument with a wavenumber resolution of 2 cm^{-1}. The temperature dependent FT-IR studies were performed in the temperature range between 25 and 85 °C. Thin-film electrolyte foils were sandwiched between two NaCl plates and placed in the FT-IR temperature-controlled cell; the accuracy of the temperature was estimated to be ±1 °C. Attenuated total reflectance (ATR) infrared spectra were recorded at 20 ± 1 °C using a Bruker IFS 66 spectrometer with a resolution of 2 cm^{-1}. For the ATR spectra, the sample was positioned on a ZnSe crystal and illuminated at a 45° angle thus allowing for multiple internal reflections.

FT-Raman Spectroscopy. FT-Raman spectra with a wavenumber resolution of 2 cm^{-1} were recorded at 25 °C with the temperature stability in the sample estimated to be ±0.3 °C. The spectra were recorded with a Bruker IFS 66 spectrometer with a Raman module (FRA 106) and a continuous Nd:YAG laser (1064 nm) using a 180° backscattering geometry. During measurements, the sample cell was placed in an evacuated thermostat.

SEM Studies. SEM studies were carried out on an Hitachi S-570 scanning electron microscope. Thin electrolyte films prepared by a solvent cast technique were mounted onto 1 cm diameter aluminum plates. Samples were sputter-graphite-coated (20 nm). All specimens were examined at a working voltage of 10 kV.

Results

Conductivity. Figure 1 presents the conductivity isotherms obtained for PEO−NNPAAM−$LiClO_4$ electrolytes at 0, 25, and 100 °C. At ambient and subambient temperatures, a considerable increase in the conductivity in comparison to the conductivity measured for the PEO−$LiClO_4$ electrolyte is observed for composite systems containing up to 30 vol % of NNPAAM. A maximum in the conductivity is found for the sample containing 15 vol % of NNPAAM. This conductivity exceeds 10^{-5} S/cm at 25 °C which is 20 times higher than for the PEO−$LiClO_4$ system at 25 °C. At 100 °C conductivities measured for the composite electrolytes are lower than for the PEO−$LiClO_4$ electrolyte.

Figure 2 presents the conductivity isotherms obtained for the OMPEO−NNPAAM−$LiClO_4$ composite electrolytes at −20, 0, 25, and 100 °C as a function of vol % of

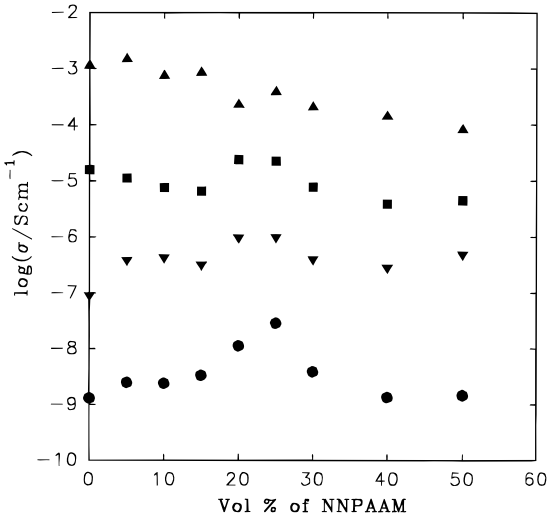

Figure 2. Isotherms of ionic conductivity of OMPEO−NNPAAM−$LiClO_4$ versus volume fraction of NNPAAM with 10 mol % $LiClO_4$: (●) −20 °C, (▼) 0 °C, (■) 25 °C, and (▲) 100 °C.

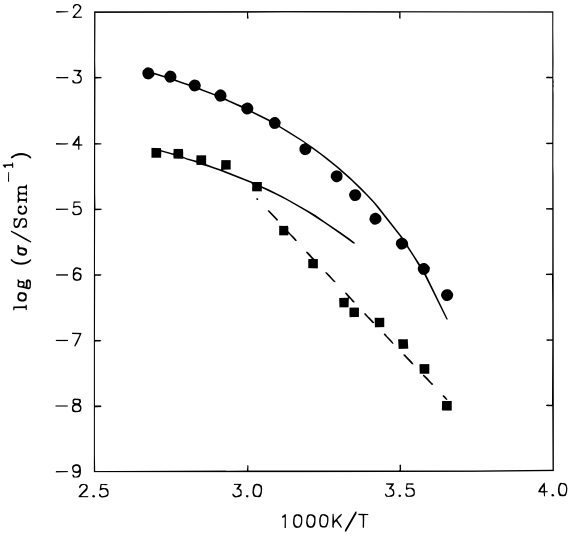

Figure 3. Ionic conductivity of PEO−NNPAAM−$LiClO_4$ with 10 mol % $LiClO_4$ as a function of inverse temperature: (●) 15 vol % NNPAAM and (■) 40 vol % NNPAAM. Solid lines display fits of eq 1 to experimental data, and the dashed line displays a fit of eq 2 to experimental data.

NNPAAM. At −20, and 0 °C conductivities measured for all of the composite systems are higher than those measured for the OMPEO−$LiClO_4$ electrolyte. A conductivity maximum is obtained for the sample containing 25 vol % of NNPAAM and is over 1 order of magnitude higher than the conductivity of the OMPEO−$LiClO_4$ electrolyte at −20 and 0 °C. At 25 °C only the conductivities measured for samples containing 20 and 25 vol % of NNPAAM are higher than those measured for the pure OMPEO−$LiClO_4$ system, whereas at 100 °C the conductivity obtained for the OMPEO−$LiClO_4$ system is the highest (see Figure 2). At this temperature a decrease in the conductivity with an increase in the NNPAAM concentration is observed. At 25 °C the conductivity decreases slightly for samples containing up to 15 vol % of NNPAAM and then reaches a maximum at 20−25 vol % of NNPAAM followed by a decrease in the conductivity for higher NNPAAM concentrations.

Figure 3 shows the temperature dependence of the conductivity for PEO−NNPAAM−$LiClO_4$ electrolytes (samples containing 15 and 40 vol % of NNPAAM). For samples containing between 15 and 25 vol % of NNPAAM, the temperature dependence of conductivity follows a VTF empirical form (eq 1) for temperatures above 55 °C. As can be seen from Figure 3 (data for the sample containing 15 vol % of NNPAAM), log σ points below 55 °C can be fit by either VTF (eq 1) or Arrhenius (eq 2) type equations. We have chosen to use a VTF form on the basis of DSC evidence which does not show the presence of a first-order transition around 55 °C for the PEO−NNPAAM−$LiClO_4$ electrolytes containing 15 and 20 vol % of NNPAAM. For samples containing higher concentrations of NNPAAM, the conductivity−temperature behavior is a mixture of Arrhenius (eq 2) (lower temperatures) and VTF (higher temperatures).

$$\sigma(T) = \frac{A}{T^{1/2}} \exp\left(-\frac{B}{k_B(T - T_o)}\right) \quad (1)$$

In eq 1 A is the conductivity preexponential factor, B is the pseudoactivation energy for conduction, T_o is the thermodynamic glass transition temperature which is usually 30−50 K lower than the glass transition temperature, T_g, determined from the DSC experiments, and k_B is the Boltzmann constant.

$$\sigma(T) = \sigma_o \exp\left(-\frac{E_a}{k_B T}\right) \quad (2)$$

In eq 2, σ_o is the conductivity preexponential factor and E_a is the activation energy for conduction.

The temperature dependence of conductivity for PEO−NNPAAM−$LiClO_4$ electrolytes has been analyzed by fitting the experimental data to eqs 1 and 2. For concentrations of NNPAAM higher than 25 vol %, the region where the ionic conductivity−temperature behavior changes from VTF to Arrhenius corresponds roughly to about 60 °C (see Figure 3), close to the melting point of PEO. The same is also true for samples containing 5 and 10 vol % of NNPAAM. The slope of the low-temperature Arrhenius curves increases with an increase in the NNPAAM concentration (for samples containing more than 25 vol % of NNPAAM) thus indicating an increase in E_a.

Figure 4 presents the temperature dependence of conductivity obtained for OMPEO−NNPAAM−$LiClO_4$ electrolytes (samples containing 5 and 30 vol % of NNPAAM). The conductivities fit the VTF form at ambient and moderate temperatures, whereas at subambient temperatures a clear deviation from VTF behavior is observed. In this temperature region the temperature dependence of conductivity follows the Arrhenius form which suggests that the conductivity is thermally activated. This is unusual for amorphous polymer electrolyte systems. A similar temperature behavior for conductivity has been found for the other OMPEO−NNPAAM systems studied. The conductivity data have been fitted to the VTF and Arrhenius equations. We have observed that generally the high-ambient and subambient temperature conductivities (see Figure 2) are associated with low E_a values calculated on the basis of eq 2.

DSC Studies. Figure 5 presents the DSC curves obtained for OMPEO (Figure 5a), the OMPEO−$LiClO_4$ electrolyte (Figure 5b), and the OMPEO−NNPAAM−$LiClO_4$ composite system (samples containing 25 and 50 vol % of NNPAAM) (Figure 5c,d). The DSC curve

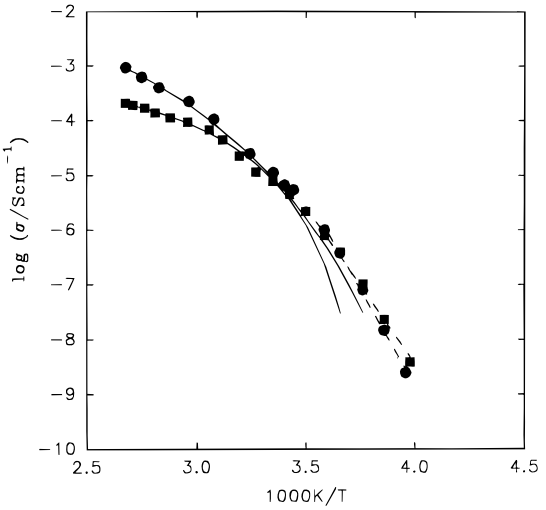

Figure 4. Ionic conductivity of OMPEO−NNPAAM−$LiClO_4$ with 10 mol % $LiClO_4$ as a function of inverse temperature: (●) 5 vol % NNPAAM and (■) 30 vol % NNPAAM. Solid lines display fits of eq 1 to experimental data, and dashed lines display fits of eq 2 to experimental data.

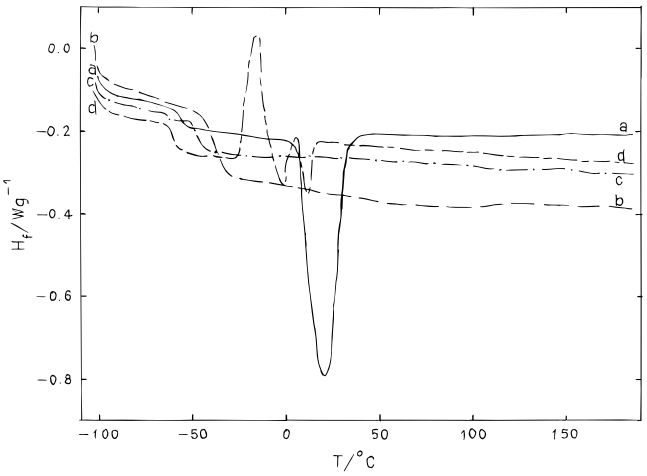

Figure 5. DSC traces obtained for OMPEO−NNPAAM−$LiClO_4$ electrolytes: (a) undoped OMPEO, (b) OMPEO−$LiClO_4$ electrolyte, (c) OMPEO−NNPAAM−$LiClO_4$ electrolyte (sample containing 25 vol % NNPAAM), (d) OMPEO−NNPAAM−$LiClO_4$ electrolyte (sample containing 50 vol % NNPAAM). Q_f is a heat flow. DSC curves were normalized to same sample mass.

registered for the pure undoped OMPEO (Figure 5a) shows a crystalline endothermic peak appearing at 10 °C and the liquid−glass transition at −58 °C. DSC results are summarized in Table 1. As can be seen in Figure 5b,c the OMPEO crystalline phase vanishes after the addition of $LiClO_4$ for samples containing up to 40 vol % of NNPAAM. In Figure 5d two endothermic peaks at −11 and 4 °C are observed for the sample containing 50 vol % of NNPAAM. The exothermic peak occurring at −33 °C on the DSC trace (Figure 5d) is connected with the recrystallization of the polyether. The DSC curves registered for composite systems containing up to 30 vol % of NNPAAM are similar to these obtained for the OMPEO−$LiClO_4$ electrolyte. For samples containing up to 25 vol % of NNPAAM, two glass transition temperatures are observed (see Figure 5c). The lower one appears in the temperature range −60 to −65 °C and is very close to the glass transition temperature of the undoped OMPEO. The higher one appears in the range −30 to −45 °C which is close to the T_g registered for the OMPEO−$LiClO_4$ electrolyte. For samples containing more than 25 vol % of NNPAAM, only one T_g is observed which decreases with an increase in the NNPAAM concentration dropping to −55 °C for the sample containing 50 vol % of NNPAAM (approaching the T_g measured for the undoped OMPEO). There is no evidence for the T_g of pure NNPAAM (∼89 °C) indicating that the NNPAAM is microphase separated. For the sample containing 40 vol % of NNPAAM, traces of crystallinity are also observed. It should be stressed that the DSC results obtained from runs 1 and 2 are very similar.

Table 1. DSC Data for OMPEO−NNPAAM−$LiClO_4$ Composite Polymeric Electrolytes

	run 1					run 2				
vol %[a]	T_{g1} (°C)	T_{g2} (°C)	T_m (°C)	Q_m (J g^{-1})	X_c (%)[b]	T_{g1} (°C)	T_{g2} (°C)	T_m (°C)	Q_m (J g^{-1})	X_c (%)[b]
0[d]	−58		10	37	18	−57		4	38	18
0	−36					−36				
5	−29	−62				−30	−52			
10	−34	−64				−31	−65			
15	−35	−61				−35	−58			
20	−44	−62				−49	−62			
25	−39	−65				−40	−55			
30	−43					−41				
40	−48		6	0.3	0.2	−49		6	0.6	0.5
50[c]	−55		−10, 9	8.5	7.9	−56		−11, 9	13.1	12.2

[a] Concentration of NNPAAM in vol %. [b] X_c has been calculated as described in the text with respect to OMPEO concentration in composite electrolyte. [c] Two numbers in the T_m column indicate onsets of two melting peaks. Q_m is calculated as a sum of melting heats for both transitions. [d] Undoped OMPEO sample.

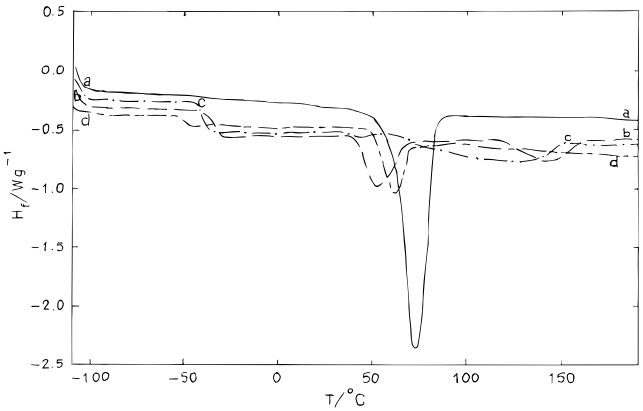

Figure 6. DSC traces obtained for PEO−NNPAAM−$LiClO_4$ electrolytes: (a) undoped PEO, (b) PEO−$LiClO_4$ electrolyte, (c) PEO−NNPAAM−$LiClO_4$ electrolyte (sample containing 15 vol % NNPAAM), and (d) PEO−NNPAAM−$LiClO_4$ electrolyte (sample containing 50 vol % NNPAAM). Q_f is a heat flow. DSC curves were normalized to same sample mass.

Figure 6 shows the DSC curves registered for the pure, undoped PEO (Figure 6a), the PEO−$LiClO_4$ electrolyte (Figure 6b), and the PEO−NNPAAM−$LiClO_4$ system (samples containing 15 and 50 vol % of NNPAAM, Figure 6c,d). The DSC parameters calculated from the DSC curves are summarized in Table 2. The addition of NNPAAM lowers the degree of crystallinity of PEO−$LiClO_4$-based electrolytes. The endothermic peak corresponding to the melting of the crystalline PEO phase is barely present for the samples containing 15 and 20 vol % of NNPAAM (see Figure 6c). For higher NNPAAM concentrations, the amount of the crystalline PEO phase increases and the position of the melting peak shifts to higher temperatures. For the sample containing 50 vol % of NNPAAM (Figure 6d), the onset temperature of the melting peak is approaching that for the undoped PEO (see Table 2). On the

Table 2. DSC Data for PEO−NNPAAM−$LiClO_4$ Composite Polymeric Electrolytes

	run 1					run 2				
vol %[a]	T_g (°C)	T_m (°C)	Q_m (J g^{-1})	X_c (%)[c]	T_{mc} (°C)[b]	T_g (°C)	T_m (°C)	Q_m (J g^{-1})	X_c (%)[c]	T_{mc} (°C)[b]
0[d]		53, 63	158	74		−53	50, 60	110	52	
0	−31	42, 54	49.5	23	105, 145	−18	43, 58	49.5	23	110, 150
5	−39	29, 37	9.6	4.7	93, 145	−37			<1	
10	−35	38, 46	5.7	3.0	74, 131	−36	49, 55	2.6	1.4	
15	−34			<1	66, 129	−32			<1	
20	−38			<1		−37			<1	
25	−37	31, 46	14	8.9		−38	30, 45	15	9.5	
30	−38	43, 57	49	32		−39	44, 58	44	30	
40	−37	47, 59	37	29		−37	47, 59	43	34	
50	−44	53, 63	46	43		−42	53, 63	52	49	

[a] Concentration of NNPAAM in vol %. [b] The first number indicates the onset temperature of the transition; the second number indicates the maximum of the transition peak. [c] X_c has been calculated as described in the text with respect to PEO concentration in composite electrolyte. [d] Undoped PEO sample.

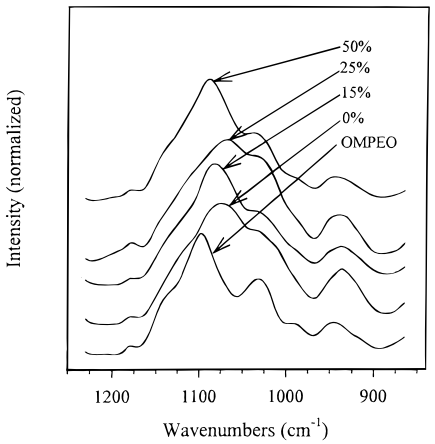

Figure 7. FT-IR spectra obtained at room temperature for the OMPEO−NNPAAM−$LiClO_4$ electrolytes.

other hand, the melting peak of the crystalline complex phase which is observed at 145 °C for the PEO−$LiClO_4$ system (Figure 6b) and PEO−NNPAAM−$LiClO_4$ electrolytes (samples containing up to 15 vol % of NNPAAM, see Figure 6c) disappears for samples of higher NNPAAM concentrations (see Figure 6d). The position of this peak shifts to lower temperatures with an increase in the concentration of NNPAAM (up to 15 vol %). The position of T_g found for composite PEO−NNPAAM−$LiClO_4$ electrolytes is slightly lower for composite systems than it is for the PEO−$LiClO_4$ electrolyte; for the sample containing 50 vol % of NNPAAM, T_g drops to −44 °C. As for the OMPEO−NNPAAM−$LiClO_4$ electrolytes, DSC results obtained for the PEO−NNPAAM−$LiClO_4$ system in runs 1 and 2 are similar. Here there is an exception for samples containing up to 15 vol % of NNPAAM where a shift of T_m to higher temperatures in run 2 is observed as compared to run 1. It can also be seen that the melting peak of the crystalline complex phase is not observed for the composite samples in run 2. This is probably due to the slow recrystallization of the complex phase which can not be completed during the fast cooling of the samples between runs 1 and 2.

FT-IR and FT-Raman Spectroscopy. Figure 7 shows a typical room temperature FT-IR spectrum obtained for polyether-NNPAAM−$LiClO_4$ electrolytes in the frequency range between 1200 and 900 cm^{-1}. The 1200−1000 cm^{-1} region corresponds to the position of the polyether C−O−C stretch bands which consist mainly of unresolved symmetric and antisymmetric vibrations. The C−O−C region shows the effect of the filler and the dopant salt on these vibrations. As can be seen from Table 3 and Figure 7, the mean position of the broad C−O−C band reaches a minimum for

Table 3. Position of the Maxima of IR Bands for OMPEO−NNPAAM−$LiClO_4$ Composite Polymeric Electrolytes at 20 °C Obtained by ATR

	type of group involved in IR vibration and position of the maximum of the IR band		
NNPAAM concentration (vol %)	C═O (NNPAAM) (cm^{-1})	C−O−C (OMPEO) (cm^{-1})	C−H, CH_2 (OMPEO) (cm^{-1})
0[a]		1100	1349
0		1074	1349
5	1637[b]	1080	1349
10	1622 (symmetric peak)	1082	1350
15	1620 (40%) 1640 (60%)	1082	1350
20	1620 (64%) 1640 (36%)	1079 (broad)	1349
25	1620 (82%) 1640 (18%)	1068 (broad)	1350
30	1620 (62%) 1640 (38%)	1072 (broad)	1349
40	1620 (50%) 1640 (50%)	1083	1350
50	1620 (70%) 1640 (30%)	1089[c]	1350
100	1640		

[a] Undoped OMPEO. [b] OMPEO has a weak vibration at 1636 cm^{-1}. [c] NNPAAM has a vibration at 1096 cm^{-1}.

samples containing 20, 25, and 30 vol % of NNPAAM and then increases with further increase in the NNPAAM concentration. The observed broadening reveals the amorphous nature of these samples.

There is a similar trend in the behavior of the C═O moiety (the 1700−1600 cm^{-1} region) which is more complex since it is part of the tertiary amide I band which we have located at 1640 cm^{-1} for dry NNPAAM. The spectral feature related to the C═O stretching vibrations contains two subbands which we interpret as being related to "free" carbonyl (∼1640 cm^{-1}) and lithium-coordinated carbonyl (∼1620 cm^{-1}). There is an interplay between the relative intensities of these two subbands (Table 3) generally indicating the relative amounts of "free" carbonyl and lithium-coordinated carbonyl as the concentration of NNPAAM increases. The amorphous character of these composite electrolytes is further confirmed by the presence of a single peak for C−H wagging vibrations appearing at 1350 cm^{-1} (see Table 3).

For the PEO−NNPAAM−$LiClO_4$ samples, a decrease in the position of the C═O mode and a slight increase in the position of the broad maximum of the C−O−C mode is observed with increase in NNPAAM concentration (see Table 4). The presence of the crystalline phase doublet in the C−H wagging mode region (1343−1360

Table 4. Position of the Maxima of IR Vibrations for PEO−NNPAAM−$LiClO_4$ Composite Polymeric Electrolytes (T = 25 °C)

NNPAAM concentration (vol %)	type of group involved in IR vibration and position of the maximum of the IR band		
	C═O (NNPAAM) (cm^{-1})	C−O−C (PEO) (cm^{-1})	C−H, CH_2 (PEO) (cm^{-1})
0[a]		1116[b]	1350
0		1092	1350
5	1646	1093	1350
10	1645	1093	1350
15	1650	1097	1350
20	1637	1096	1350
25	1633	1098	1349
30	1628	1099	1343−1360
40	1623	1101	1343−1361
50	1623	1107	1343−1360
100	1640		

[a] Undoped PEO. [b] A spectrum obtained above the melting point of the crystalline PEO phase.

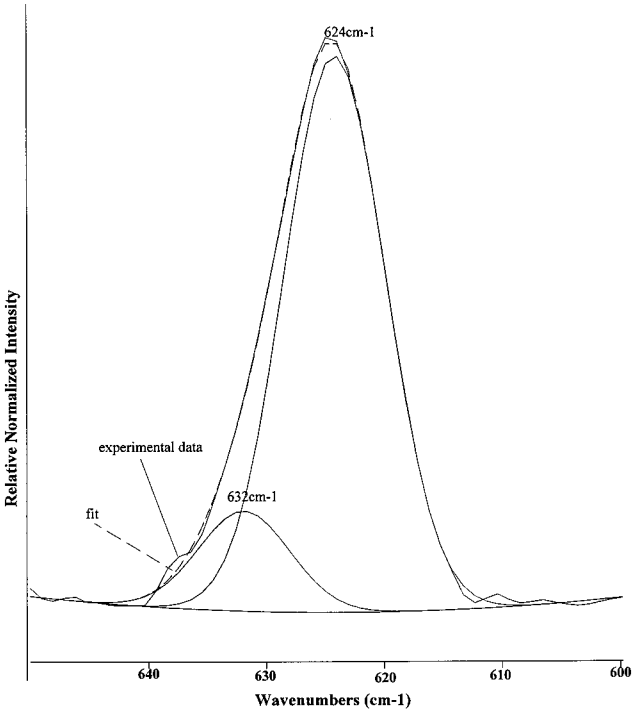

Figure 8. Peak fitting for the $\nu(ClO_4^-)$ FT-IR region for the PEO−NNPAAM (10 vol %)−$LiClO_4$ sample at 25 °C.

cm^{-1}) is noted for the samples for which a significant amount of the crystalline PEO phase has been found in the DSC experiments described above.

A Galactic Grams 386 software package was used to separate the $\nu(ClO_4^-)$ mode into two contributions with maxima in the 620−624 and 630−635 cm^{-1} ranges. An example of this separation is shown in Figure 8 for the PEO−NNPAAM (10 vol %)−$LiClO_4$ sample. Salomon et al. suggest that [17] the $\nu(ClO_4^-)$ band centered at 623 cm^{-1} can be attributed to spectroscopically "free" ClO_4^-, whereas the band centered between 630−635 cm^{-1} is associated with the presence of contact ion pairs.

The "free" anion and contact ion pair bands have been fitted from the raw FT-IR data. The fractions of "free" anions and contact ion pairs have been calculated as the ratio of the area under the peaks attributed respectively to "free" anions and contact ion pairs to the total area for the $\nu(ClO_4^-)$ vibrations. All band areas were normalized to the CH_2 stretch of polyethers. The results are shown in Figure 9 for the PEO−NNPAAM−$LiClO_4$ and OMPEO−NNPAAM−$LiClO_4$ systems. In Figure 9 the fraction of "free" anions is plotted against the concentration of NNPAAM. For the OMPEO−NNPAAM−$LiClO_4$ system, the fraction of "free" ions is very high for samples containing more than 5 vol % of NNPAAM. For the PEO-based electrolytes containing up to 15 vol % of NNPAAM, the fraction of "free" ions is similar to that found for the PEO−$LiClO_4$ electrolyte. For the higher concentration of NNPAAM, the fraction of "free" ions is more than 90%. We have also observed that the fraction of ion pairs increases with an increase in temperature.

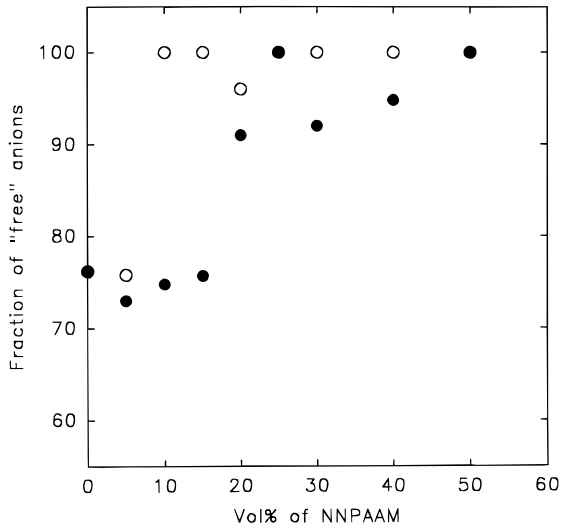

Figure 9. Changes in the fraction of "free" ClO_4^- anions as a function of NNPAAM concentration (vol %) for (○) OMPEO−NNPAAM−$LiClO_4$ composite electrolytes and (●) PEO−NNPAAM−$LiClO_4$ composite electrolytes. Data were obtained on the basis of FT-IR spectra recorded at 25 °C.

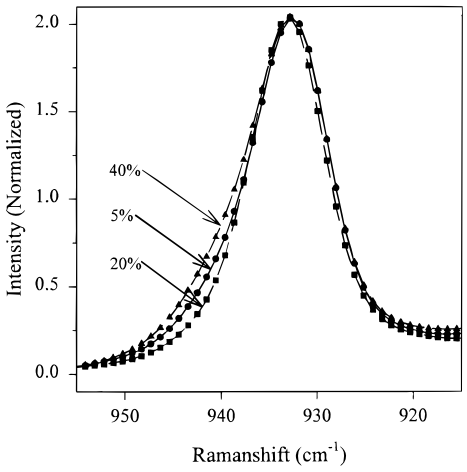

Figure 10. Raman intensity (normalized to the 932 cm^{-1} ClO_4 symmetric stretch peak) plotted versus the frequency shift for OMPEO−NNPAAM−$LiClO_4$ composite electrolytes of various NNPAAM concentrations.

Support for the interpretation that the relative amount of free charge carriers increases to a maximum with the concentration of NNPAAM increasing to 20 vol % of NNPAAM is also given by the FT-Raman data of the ClO_4^- symmetric stretch. According to previous assignments,[18] the band at 932 cm^{-1} corresponds to the "free" perchlorate anion which is shifted to 939 cm^{-1} for $Li^+ClO_4^-$ contact ion pairs. As seen in Figure 10, the bandwith of the ClO_4^- symmetric stretch decreases slightly with increasing concentration of NNPAAM to a minimum for 20 vol % whereafter it increase, the

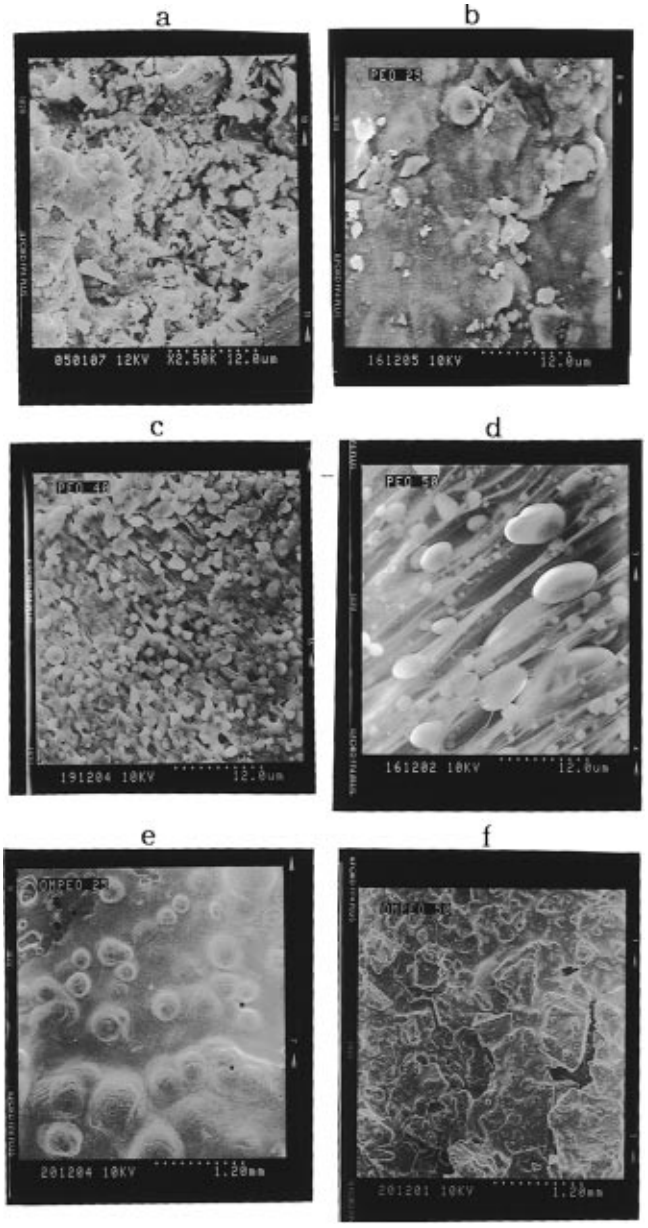

Figure 11. SEM photographs obtained for PEO−NNPAAM−$LiClO_4$ composite electrolytes containing (a) 0 vol % NNPAAM, (b) 25 vol % NNPAAM, (c) 40 vol % NNPAAM, and (d) 50 vol % NNPAAM and for OMPEO−NNPAAM−$LiClO_4$ composite electrolytes containing (e) 25 vol % NNPAAM and (f) 50 vol % NNPAAM. (Figure was reduced to 67% of original size for publication.)

change occurring on the high-frequency side of the band. This result indicates that the relative amount of ion pairs is reduced upon complexation with the NNPAAM. The observed initial decrease in bandwith with increased vol % of NNPAAM is further accentuated by the fact that the Raman spectrum of pure NNPAAM exhibits a broad feature at ~940 cm^{-1} which would increase the bandwith of this spectral feature if the fraction of contact ion pairs was constant.

SEM Studies. Figure 11 presents SEM photographs obtained for the PEO−$LiClO_4$ electrolyte (part a) and PEO−NNPAAM−$LiClO_4$ composite electrolytes (parts b−d). Figure 11c,d shows a homogenous distribution of NNPAAM fillers for samples containing respectively 40 and 50 vol % of NNPAAM. These two pictures also show that the structure of these composite samples differs from those found for the PEO−$LiClO_4$ electrolyte (see Figure 11a) and the PEO−NNPAAM−$LiClO_4$ electrolyte (25 vol % of NNPAAM, see Figure 11b). The well-defined crystalline PEO lamellae are clearly seen in Figure 11c,d, whereas Figure 11a,b indicates a rather amorphous structure for the respective electrolytes. The thickness of PEO lamellae increases with an increase in the NNPAAM concentration; compare Figure 11, parts c and d which have the same magnification.

SEM photographs were also obtained for OMPEO−NNPAAM−$LiClO_4$ electrolytes containing 25 and 50 vol % of NNPAAM. The sample containing 50 vol % of NNPAAM (see Figure 11f) has much more structure than the one with 25 vol % (see Figure 11e). The SEM studies are in good agreement with the DSC data presented in Tables 1 and 2 and the FT-IR data presented in Tables 3 and 4, confirming that changes in the structure and morphology of polyether−NNPAAM−$LiClO_4$ electrolytes can be correlated with changes in the NNPAAM concentration.

Discussion

From the conductivity results above, it can be concluded that the addition of NNPAAM to both PEO−$LiClO_4$ and OMPEO−$LiClO_4$ electrolytes enhances their ambient and subambient temperature ionic conductivities. Similar to previous studies on the polyether−PAAM−$LiClO_4$ system,[9] we can attribute the changes in the electrolyte conductivity to Lewis acid−base type interactions of the polyether matrices and NNPAAM with $LiClO_4$ leading to the formation of various types of complexes. Three types can be distinguished.

Type I Complexes: polyether−Li^+−polyether complexes involving Lewis base ether oxygens from the polyether chain. These complexes incorporate transient cross-links between the polyether chains via alkali metal cations which stiffen the polyether host and reduce the electrolyte conductivity. These cross-links can be either intra- or intermolecular.[19−21]

Type II Complexes: mixed polyether−Li^+−NNPAAM complexes involving Lewis base ether oxygens from the polyether chain and Lewis base carbonyl oxygens from the NNPAAM chain. The possibility of the formation of complexes involving polyamide nitrogen has been mentioned in earlier studies.[22,23] In our system changes in the nitrogen environment with changes in NNPAAM concentration were found to be negligible from FT-IR studies, whereas the coupling of Li^+ cations to carbonyl oxygens is demonstrated by the shift of the C═O band to lower frequencies for composite systems containing NNPAAM (see Tables 3 and 4). Therefore we conclude that Li^+ is preferentially coupled to Lewis base oxygen centers of the NNPAAM molecule.

Type III Complexes: NNPAAM−Li^+−NNPAAM complexes involving the Lewis base carbonyl oxygens of NNPAAM. These cross-links can be either intra- or intermolecular.

These three complexes are schematically shown in Figure 12. Complexes of similar schematic structure have been previously reported by Li and Khan[24] for PEO−poly(2(or 4)-vinylpyridine)−$LiClO_4$ systems.

The formation of the type II and III complexes leads to a lowering of the concentration of the type I complexes and therefore to a reduction in the density of transient cross-links. This is manifested for the OMPEO−NNPAAM−$LiClO_4$ electrolytes by the presence of a highly flexible polyether phase with a T_g comparable to that of the undoped OMPEO. The presence of this phase is probably the reason for an increase in the ionic conductivity of the composite OMPEO−NNPAAM−

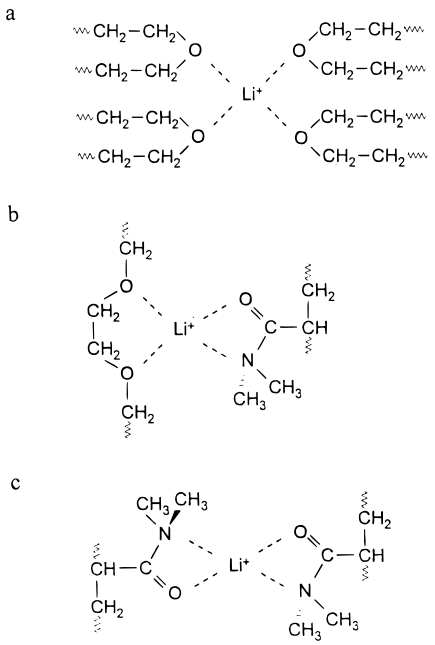

Figure 12. Schematic structure of the complexes formed by Li^+ cation with (a) polyether chains (type 1 complexes), (b) polyether and NNPAAM chains (type II complexes), and (c) NNPAAM chains (type III complexes).

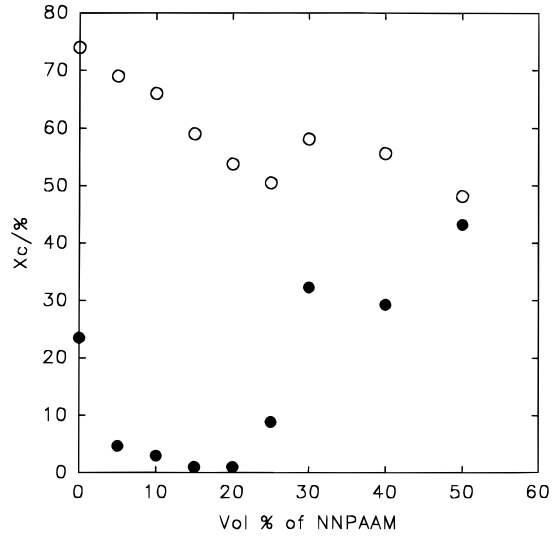

Figure 13. Degree of crystallinity, X_c, versus NNPAAM concentration (vol %) for PEO−NNPAAM blends: (○) undoped PEO−NNPAAM blends and (●) PEO−NNPAAM−$LiClO_4$ composite electrolytes.

$LiClO_4$ electrolytes in comparison with the OMPEO−$LiClO_4$ system. In the case of the PEO−NNPAAM−$LiClO_4$ electrolytes, the second, low-temperature T_g is not observed; this is probably due to the higher degree of crystallinity (X_c) of the PEO-based electrolytes. However a reduction in X_c for the PEO−$LiClO_4$ system after the addition of NNPAAM is clear. Also a decrease in T_g for composite electrolytes in comparison to the PEO−$LiClO_4$ system is observed (see Table 2).

In Figure 13 changes in X_c for the PEO−NNPAAM−$LiClO_4$ electrolytes and the undoped PEO−NNPAAM blends are plotted as a function of NNPAAM concentration and compared to those obtained respectively for the PEO−$LiClO_4$ electrolyte and undoped PEO. X_c has been calculated as a ratio of the heat of melting of the crystalline PEO phase to the heat of melting of the pure crystalline PEO (213 J/g).[16] The heat of melting of the crystalline PEO−$LiClO_4$ complex phase was neglected. As can be seen the X_c obtained for undoped blends is only slightly lower than that for the pure PEO. A larger difference is observed between values of X_c for the composite PEO−NNPAAM−$LiClO_4$ system and the PEO−$LiClO_4$ electrolyte for NNPAAM concentrations lower than 25 vol %. It can be assumed that the presence of the complexes types II and III, which can act as crystallization retarders, leads to the distortion of the crystalline PEO structure. Hence the observed changes in X_c also result from the Lewis acid−base interactions in the composite electrolyte.

The formation of various types of complexes is confirmed by the DSC data obtained for the PEO−NNPAAM−$LiClO_4$ composite electrolytes. For NNPAAM concentrations lower than 15 vol %, the presence of the crystalline PEO−$LiClO_4$ complex phase is observed together with the presence of traces of the pure crystalline PEO phase. The observed lowering of the onset temperature of the melting peak of the crystalline PEO−$LiClO_4$ complex follows changes in the morphology of this phase, especially following a decrease in spherulite size. The PEO−NNPAAM−$LiClO_4$ composite electrolyte containing 20 vol % of NNPAAM is completely amorphous, whereas for samples of higher NNPAAM concentration an increase in the fraction of the pure crystalline PEO phase is observed. A similar trend is found for OMPEO−NNPAAM−$LiClO_4$ electrolytes for which traces of the crystalline OMPEO phase are seen for samples containing 40 and 50 vol % of NNPAAM. These observations suggest strong interactions between Li^+ and carbonyl oxygens of NNPAAM confirmed by the changes in the lithium-coordinated C═O IR absorption band at ∼1620 cm^{-1}. In comparison with the "free" carbonyl band at 1640 cm^{-1}, this band has a maximum intensity for the OMPEO−NNPAAM−$LiClO_4$ electrolyte with 25 vol % of NNPAAM. Thus the lithium cation has been drawn into the NNPAAM regions increasing the flexibility of the polyether and maximizing the conductivity as observed. The 50 vol % sample (Table 3) is anomalous and indicates a departure from the earlier trend. In the case of the PEO-based composite electrolytes, we were unable to separate out the 1620 and 1640 cm^{-1} subbands, but the overall trend leads to the decrease in the position of the C═O band with an increse in the NNPAAM concentration. This decrease is significant and confirms strong coupling of Li^+ cation with NNPAAM which for samples containing 40 and 50 vol % of NNPAAM results in lower ambient temperature conductivities comparable to the conductivity measured for the PEO−$LiClO_4$ electrolyte. The interactions between NNPAAM and Li^+ cations are even more significant at temperatures around 100 °C, leading to a reduction in the conductivity of the composite electrolytes in comparison to the pure polyether-based systems (see Figure 1).

The formation of various types of complexes is also confirmed by the FT-IR data in the C−O−C stretch region. Initial shifts of the C−O−C stretch to lower frequencies observed for the OMPEO-based composite electrolytes are connected with the formation of the type II complexes which further weaken the C−O−C bonds. An increase in the frequency of the C−O−C stretch observed for both the OMPEO−NNPAAM−$LiClO_4$ and PEO−NNPAAM−$LiClO_4$ systems for NNPAAM concentrations higher than 30 vol % is due to the formation of the type III complexes reducing the concentration of the type I and II complexes and therefore changing the environment of the polyether oxygens. The strong

coupling of the Li^+ cations to the NNPAAM carbonyl oxygens is also confirmed by a reduction in the fraction of contact ion pairs found from the FT-IR data. It is possible that NNPAAM produces a steric hindrance in the coordination sphere of Li^+ thus making it difficult to form $Li^+ClO_4^-$ contact ion pairs; an increase in the number of Lewis bases per unit volume could also reduce the number of contact ion pairs. Changes in the fraction of contact ion pairs observed for the PEO−NNPAAM−$LiClO_4$ electrolytes correlate with the DSC data. For samples for which the formation of the PEO−$LiClO_4$ complex phase is seen from the DSC data (e.g., up to 15 vol % of NNPAAM), there is no significant reduction in the fraction of contact ion pairs. For the higher NNPAAM concentrations, the PEO−$LiClO_4$ complex vanishes and a significant reduction in the fraction of contact ion pairs is observed (see Figures 6 and 9).

Changes in the morphology of the composite systems are confirmed by SEM studies. For the PEO−NNPAAM−$LiClO_4$ electrolytes (samples containing 40 and 50 vol % of NNPAAM), crystalline PEO lamellae are observed which confirms crystallization of PEO chains. Also the OMPEO−NNPAAM (50 vol %)−$LiClO_4$ sample which has the highest degree of crystallinity among the OMPEO−NNPAAM−$LiClO_4$ composite polymeric electrolytes displays higher ordering in comparison with other OMPEO-based composite electrolytes as observed by SEM studies (see Figure 11e,f).

So far the properties described for amorphous (e.g., OMPEO-based) or semicrystalline (e.g., PEO-based) composite electrolytes containing NNPAAM as an additive are similar. Some differences in the behavior of both systems can be found in Figures 3 and 4 displaying the temperature dependence of their ionic conductivity. For the semicrystalline PEO−NNPAAM−$LiClO_4$ electrolytes (samples containing less than 15 and more than 20 vol % of NNPAAM), the temperature dependence of the conductivity follows an Arrhenius form for the temperature region below the melting point of the crystalline PEO phase and a VTF form for temperatures above (see Figure 3). As mentioned above the slope of the conductivity curve (in the Arrhenius region) increases both with an increase in the concentration of NNPAAM (for samples containing more than 25 vol % of NNPAAM) and with an increase in the concentration of the pure crystalline PEO phase. This can be connected to the presence of a nonconductive phase and therefore to a higher thermal activation energy being required for conduction.

The conductivity of amorphous OMPEO−NNPAAM−$LiClO_4$ composite electrolytes displays a VTF temperature dependence (see Figure 4). However for all of the samples studied, a deviation from the VTF curve at temperatures slightly above T_g (usually in the region $1.2-1.4T_g$) is observed. Below this temperature range the temperature dependence of the conductivity is more Arrhenius in spite of the fact that the systems studied are nearly amorphous. It should be stressed that in this temperature region conductivities measured for all the OMPEO−NNPAAM−$LiClO_4$ composite electrolytes are higher than for the pure OMPEO−$LiClO_4$ electrolyte. An Arrhenius type temperature dependence of the conductivity implies that in the temperature region below $1.2-1.4T_g$ the conductivity of amorphous composite electrolytes is a result of thermally activated hopping. This change in the mechanism of conduction is reminiscent of the behavior now under intense discussion for glass-forming liquids. Gotze and Sjorgen[25] review the development of a theory for the liquid−glass transition in which the generalized Boltzmann equation is solved using a mode-coupling approximation. This mode-coupling theory (MCT) predicts a change in the dynamics of the liquid at a critical crossover temperature ($T_C > T_g$) around which there is a change in diffusion mechanism. Above T_C an atomic particle interacts simultaneously with up to 10 or more nearest neighbors and diffuses as this "cage" opens and closes due to the locally coupled longitudinal density and current fluctuations in this collective medium; there is no potential barrier, and density fluctuations alway decay to zero. Below T_C, in its idealized form, the MCT envisages the particles of the fluid as being permanently trapped in cages formed by their neighbors. Because particles have no chance to escape, density fluctuations no longer totally decay. The idealized version over emphasizes the tendency of the fluid to freeze, and inclusion of thermally activated hopping restores ergodicity in the region of T_C. Activated (e.g., Arrhenius) processes are required for diffusion as the "cage" becomes a cavity for the trapped particle which must "hop" over or "through" a potential barrier to diffuse. This crossover occurs for viscosities $\eta \sim 10^2$ Poise or relaxation times of $\sim 10^{-9}$ s.

Following the discussion given above, it is noted that there is a change in the conduction mechanism at temperatures in the range $1.2-1.4T_g$. Above this temperature, which might be indentified with the MCT T_C, the motion of ions is coupled to segmental structural relaxation of the polyether chain segments. Below this temperature, ionic motion is a result of activated hopping and is largely decoupled from segmental motion. An increase in conductivity measured below $\sim 1.2T_g$ for composite systems compared to basic polyether−$LiClO_4$ electrolyte may be due to the creation of new sites available for hopping. This is consistent with the creation of different types of complexes when formation of the type II and III complexes reduces the number of cations attached to the polyether chain, thus creating ether oxygens available for coordination with relaxing cations. Therefore in this temperature range conductivity occurs via a hopping mechanism involving jumps of Li^+ cations between available (uncomplexed) polyether oxygens. It has been shown recently[26,27] that for the temperature range below $\sim 1.2\ T_g$ the contribution of the cation to ionic conductivity becomes more significant than above $\sim 1.2T_g$ where anions are the dominant mobile species.

Effective Medium Theory Model: Theoretical Background. The EMT approach for nonconductive dispersoids is based on an improved concept developed originally by Nan and Smith for composite solid electrolytes.[28,29] This approach has currently been modified by us and used to model conductivity data for several composite polymeric electrolytes.[9,10] The development of our EMT model has been extensively discussed elsewhere.[9,10,30] Below a general overview of the model is presented.

The model connects an enhancement of conductivity with the existence of a highly conductive amorphous layer at the polymer−filler interface. This layer exhibits a conductivity considerably higher than that for the matrix polymer electrolyte. Therefore in composite electrolytes there are three phases with different electrical properties (see Figure 14). These are (1) the highly conductive uncomplexed polyether interface layers surrounding the NNPAAM core (component 1 in

Figure 14. Schematic drawing of the morphology of composite polyether−NNPAAM electrolytes (see text).

Figure 14), (2) the dispersed insulating NNPAAM−$LiClO_4$ or polyether−NNPAAM−$LiClO_4$ type III or II complexes (component 2 in Figure 14), and (3) the matrix polymer ionic conductor (from the OMPEO−$LiClO_4$ or $(PEO)_{10}LiClO_4$ system) (component 3 in Figure 14). In the first step we consider components 1 and 2 as a composite unit and calculate the conductivity of this unit, σ_c, according to the Maxwell−Garnett mixture rule.

$$\sigma_c = \sigma_1 \frac{2\sigma_1 + \sigma_2 + 2Y(\sigma_2 - \sigma_1)}{2\sigma_1 + \sigma_2 - Y(\sigma_2 - \sigma_1)} \quad (3)$$

Here σ_1 and σ_2 are respectively the conductivities of the components 1 and 2 (see Figure 14). Y is the volume fraction of NNPAAM in each composite unit calculated as

$$T = \frac{1}{\left(1 + \frac{t}{R}\right)^3} \quad (4)$$

where t is the thickness of the interface layer, R is the radius of the filler grain, and spherical symmetry has been assumed (see Figure 14).

According to the above consideration, the composite electrolyte can be treated as a quasi-two-phase mixture consisting of a polymeric ionic conducting matrix (component 3) with dispersed composite units. Therefore after introducing improved conductivity parameters, calculated according to the method proposed by Nakamura[31] or Nan and Smith,[28,29] into the self-consistent EMT equation suggested by Kirkpatrick,[32] we obtain

$$\frac{V_2}{Y}\frac{\sigma_c - \sigma_m}{\sigma_c + \left(\frac{1}{p_c} - 1\right)\sigma_m} + \left(1 - \frac{V_2}{Y}\right)\frac{\sigma_e - \sigma_m}{\sigma_e + \left(\frac{1}{p_c} - 1\right)\sigma_m} = 0 \quad (5)$$

In eq 5 σ_m is the conductivity of the composite polymeric electrolyte system, p_c (=0.28[28,29]) is a continuous percolation threshold for the composite units which are allowed to overlap, σ_e is the conductivity of the matrix polymeric electrolyte, and V_2 is the volume fraction of the dispersed filler in the bulk electrolyte.

According to eq 5 the largest enhancement of ionic conductivity is obtained when the composite units fill the total volume of the electrolyte. This occurs for a special value ($V_2^* = Y$. For dispersed filler concentrations exceeding V_2^*, the quasi-two-phase system consists of a mixture of composite units and dispersed bare insulating grains and no polymer electrolyte other than that in composite units. For this case eq 5 should be rewritten in the following form:[28,29]

$$\frac{(1 - V_2)(\sigma_c - \sigma_m)}{\sigma_m + P_c(\sigma_c - \sigma_m)} + \frac{(V_2 - V_2^*)(\sigma_2 - \sigma_m)}{\sigma_m + P_c(\sigma_2 - \sigma_m)} = 0 \quad (6)$$

P_c is the percolation threshold of the dispersed bare insulating grains which are not allowed to overlap. Therefore P_c is different from p_c (see eq 5) and was taken as the percolation threshold for a general random mixture, equal to 0.15.[28,29]

Since the structure of the interface layer is highly amorphous, it is assumed in what follows that the temperature dependence of its conductivity (σ_1) would follow eq 1. It was also assumed, for the calculation of the σ_1 as a function of the filler concentration, that the pseudoactivation energy B and the preexponential factor σ_o were independent of the dispersed filler concentration. Therefore the interface layer conductivity is only dependent on T_o and decreases with an increase in T_g. Values of T_g were taken from DSC measurements and used for the calculation of σ_1 for electrolytes with various concentrations of the NNPAAM.

To generalize our model the variation of T_g as a function of grain size and concentration should be considered. It was found that a good fit is obtained when T_g is approximated by

$$T_g = K_o + K_1 V_2 + K_2 V_2^2 \quad (7)$$

In this equation (used in fitting our data) the effect of the salt is included in K_o which for the PEO−NNPAAM−$LiClO_4$ composite electrolytes is identical to T_g for the pristine polymeric electrolyte with no dispersed phase. For the OMPEO−NNPAAM−$LiClO_4$ electrolytes, K_o corresponds roughly to the T_g of the undoped OMPEO. K_1 describes the influence of the added filler on the T_g of the composite system, and K_2 is connected with the polymer−filler−salt interaction.

Finally in this model the conductivity (σ_1) of the component 1 in Figure 14 has been calculated using eq 1 in which values of T_o are related to the T_gs calculated from eq 7. (The data used for the EMT calculations are summarized in Table 5.) σ_1 obtained from eq 1 is then introduced into eq 3, and the conductivity of the

Table 5. Parameters Used for Calculations of Temperature and Composition Dependence of the Conductivity of Composite OMPEO−NNPAAM−$LiClO_4$ and PEO−NNPAAM−$LiClO_4$ Polymeric Electrolytes Using EMT Models

kind of phase	A (S $K^{0.5}$ cm^{-1})	T_o (K)	Bk_B^{-1} (K)
OMPEO−$LiClO_4$	26.97	195.0	1204.0
PEO−$LiClO_4$[b]	160.6	203.0	1405.0
surface layer (OMPEO-based electrolytes)	26.97	T_g − 30 K	1204.0
surface layer (PEO-based electrolytes)	26.97	T_g − 50 K	1204.0

[a] For VTF parameters, see eq 1. [b] Calculated form the temperature dependence of conductivity above the melting point of the crystalline PEO phase. It has been assumed that the conductivity of component 2 is temperature independent and equal to 10^{-12} S/cm as measured by us for NNPAAM−$LiClO_4$ (10 mol %) electrolyte at ambient temperatures. The T_g of the surface layer has been calculated on the basis of eq 7 using the following parameters: $K_o = 223.5$, $K_1 = -82.2$, and $K_2 = 172.1$ for OMPEO−NNPAAM−$LiClO_4$ electrolytes and $K_o = 240.5$, $K_1 = -20.2$, and $K_2 = 2.3$ for PEO−NNPAAM−$LiClO_4$ electrolytes. The conductivity of PEO−$LiClO_4$ electrolyte below the melting point of the crystalline PEO phase has been calculating using eq 2 with E_a = 126 kJ/mol and $\sigma_o = 9.62 \times 10^{15}$ S cm^{-1}.

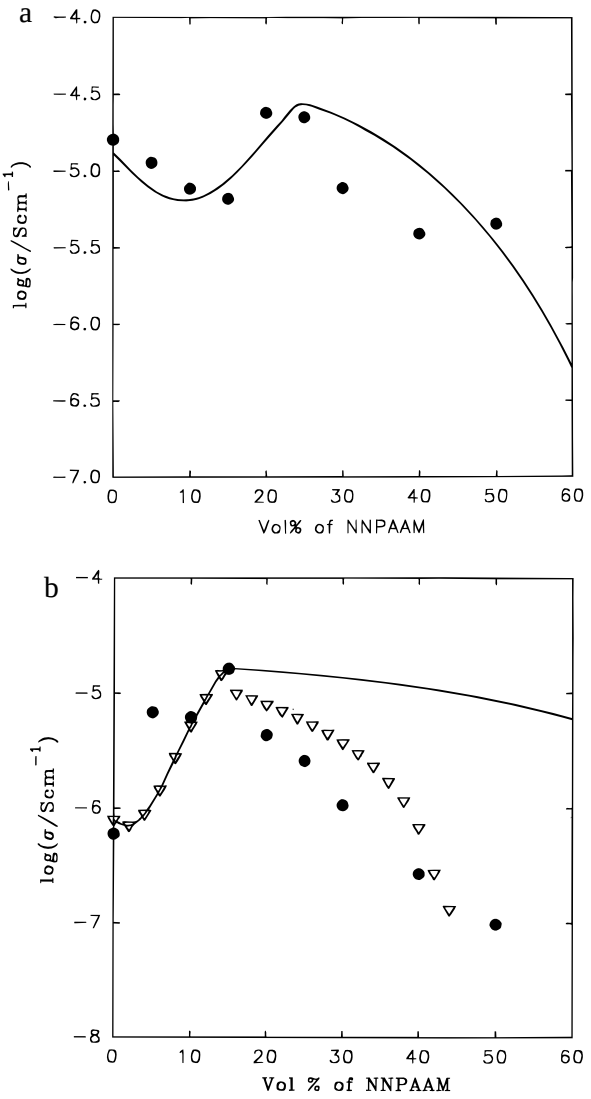

Figure 15. Comparison of the experimentally measured isothermal conductivities (T = 25 °C) with theoretically calculated conductivities on the basis of the EMT model. Data are presented for (a) OMPEO−NNPAAM−$LiClO_4$, (●) experimental data and (—) theoretical, and (b) PEO−NNPAAM−$LiClO_4$, (●) experimental data and (—) theoretical; (▽) theoretical (corrected model, see text).

composite unit is calculated. The conductivity of component 2 was assumed to be temperature independent and measured as equal to 10^{-12} S/cm at room temperature. The total conductivity of composite electrolytes is calculated on the basis of eq 5 or 6 depending on the filler concentration range. For the calculation of the temperature dependence of the ionic conductivity, it has been assumed that the conductivity of component 1 follows eq 1. The temperature dependence of the conductivity of the OMPEO−$LiClO_4$ electrolyte also follows eq 1, whereas for the calculation of the temperature dependence of the conductivity for the PEO−$LiClO_4$ electrolytes, eq 2 is used below T_m and eq 1 above. All the parameters used for these calculations are summarized in Table 5. The method of calculation of the t/R ratio as a function of the NNPAAM concentration in PEO−NNPAAM−$LiClO_4$ electrolytes is the same as previously used for PEO−PAAM−$LiClO_4$ systems[9]. The t/R ratio used in EMT calculations was equal to 0.6.

Figure 15 presents EMT fitting of the isothermal room temperature conductivities (T = 25 °C) for the OMPEO−NNPAAM−$LiClO_4$ electrolytes (Figure 15a)

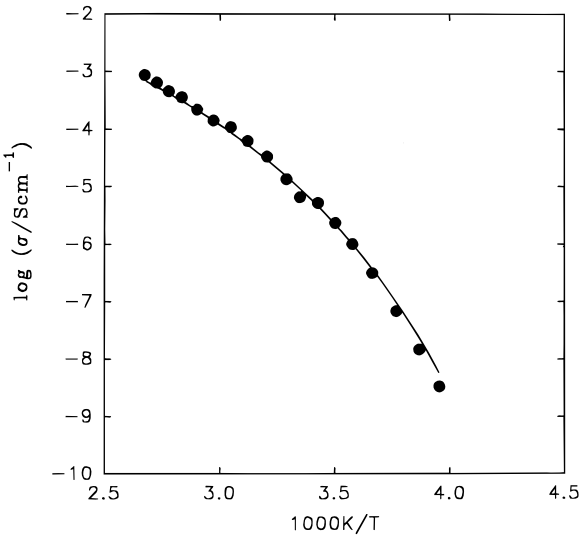

Figure 16. Comparison of the experimentally measured (●) temperature dependence of conductivity for OMPEO−NNPAAM−$LiClO_4$ electrolyte (15 vol % NNPAAM) with theoretical temperature dependence of conductivity calculated on the basis of the EMT model (solid lines).

and the PEO−NNPAAM−$LiClO_4$ electrolytes (Figure 15b). A comparison is made between the experimental data and calculations on the basis of the EMT approach (solid lines). As can be seen (Figure 15a) there is a reasonable fit of the model up to 25 vol % of NNPAAM. A difference is observed between the experimental data and the model for samples containing 30 and 40 vol % of NNPAAM. We suggest that this is the result of strong interactions between Li^+ cations and NNPAAM leading to the immobilization of Li^+ cations and hence the reduction in the charge carrier density in the conductive phase. Since the EMT model does not predict the Lewis acid−base interactions, the conductivity calculated from the model in this NNPAAM concentration range is considerably higher than the measured data. This difference between experiment and model is even more apparent in Figure 15b. For PEO−NNPAAM−$LiClO_4$ electrolytes, the model fits conductivity data only up to the maximum in the conductivity observed at an NNPAAM, concentration of 15 vol %. For higher concentrations of NNPAAM experimentally measured conductivities fall below the model. This behavior is due to the coupling of the Li^+ cations to the Lewis base centers in the NNPAAM chain which leads to the formation of a considerable quantity of an undoped, nonconductive PEO phase. Therefore in addition to the presence of the bare insulating NNPAAM−$LiClO_4$ phase, an additional nonconductive PEO phase is present which is not predicted by our EMT model. To modify our model we suggest that for concentrations of NNPAAM exceeding V_2* the addition of each NNPAAM molecule causes the creation of an equivalent amount of volume fraction of an nonconductive, undoped PEO phase. This would insert the value $2V_2$ in eq 6 instead of V_2 as the volume fraction of the dispersed insulating phase. The results of calculations based on these modifications are shown as triangles in Figure 15b. The new model qualitatively predicts the abrupt decrease in the conductivity of the OMPEO−NNPAAM−$LiClO_4$ electrolytes after approaching the conductivity maximum. However, there are still quantitative differences between experiment and EMT model.

Figure 16 presents a comparison between the experimentally obtained temperature dependence of the con-

ductivity and data calculated on the basis of the EMT approach for the OMPEO−NNPAAM (15 vol %)-$LiClO_4$. A similar fit is obtained for the PEO−NNPAAM−$LiClO_4$ systems and other OMPEO−NNPAAM−$LiClO_4$ systems. Experiment and model are in good agreement over the entire temperature range studied.

Semiempirical Conductivity Relations. For systems for which the temperature dependence of the conductivity follows eq 2, the order−disorder temperature (T_D) is the temperature at which a change in the conduction mechanism is expected. T_D can be calculated on the basis of a semiempirical approach described below. The preexponential factor (σ_o) in eq 2 can be described as follows

$$\sigma_o = K_t \omega_o \exp \frac{S_a}{k} \tag{8a}$$

where

$$K_t = \frac{Ng^2a^2zc(1-c)}{6fkT} \tag{8b}$$

K_t is the theoretical cation and anion charge carrier concentration term. The term $z(1 - c)$ is the fraction $(1 - c)$ of the z nearest neighbor energetically equivalent sites that are empty, c is the fraction of the nearest neighbor energetically equivalent sites that are occupied, a is the jump distance between energetically equivalent sites, N is the density of energetically equivalent sites, q is an electronic charge, T is the temperature in kelvin, f is a correlation factor, ω_o is an ionic oscillation frequency, and S_a is the activation entropy for conduction.

Rewriting eq 8a we find that

$$\ln \sigma_o = \frac{S_a}{k} + \ln K_t \omega_o \tag{9}$$

For many materials S_a and E_a are related by the following equation,

$$\frac{E_a}{T_D} = S_a \tag{10}$$

This equation was originally developed by Dienes to describe atomic diffusion in metals.[33] For metals T_D represents the melting point, but for fast ionic conductors this temperature usually corresponds to order−disorder transitions in the electrolyte. By combining eqs 9 and 10, eq 11 can be obtained; this will provide a method for calculating T_D for the temperature region in which the electrolytes obey the Arrhenius equation.

$$\ln \sigma_o = \frac{E_a}{kT_D} + \ln K_t \omega_o = \alpha E_a + \beta \tag{11}$$

where $\alpha = 1/kT$ and $\beta = \ln K\omega_o$. Eq 11 has recently been used to describe the correlation between preexponential factors and activation energies calculated from eq 2 for various solid ionic conductors.[34]

Figure 17 plots ln σ_o versus E_a for the subambient temperature region for OMPEO−NNPAAM−$LiClO_4$ electrolytes (Figure 17a) and the ambient temperature region for PEO−NNPAAM−$LiClO_4$ electrolytes (Figure 17b; samples containing less than 15 and more than 20 vol % of NNPAAM). In both cases a linear relation between ln σ_o and E_a is found. The order−disorder

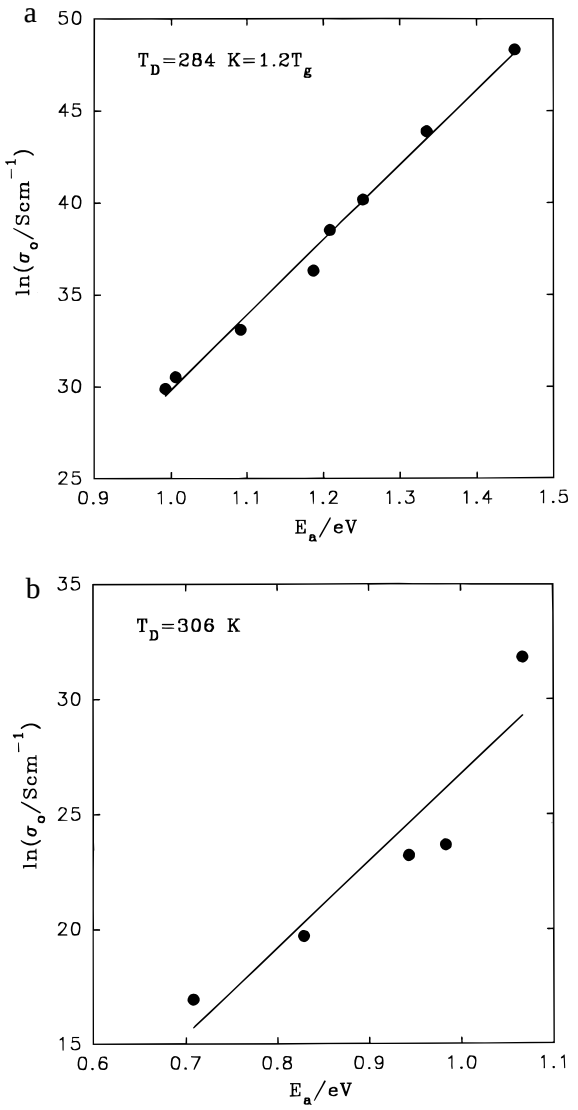

Figure 17. ln σ_o versus E_a obtained for (a) OMPEO−NNPAAM−$LiClO_4$ electrolytes and (b) PEO−NNPAAM−$LiClO_4$ electrolytes; (●) experimental data; solid line fit to eq 11.

temperature calculated for the OMPEO based composite electrolytes is equal to 284 K which is equal to 1.2 times the T_g found for the OMPEO−$LiClO_4$ electrolyte (see Table 1). This result highlights the change in the conduction mechanism indicated above and draws attention to similarities with the MCT. On the basis of this calculation, it can be assumed that T_D (=T_C) is a characteristic temperature for any group of polymeric electrolytes based on the same polymer matrix. Therefore it describes properties of the polymer matrix rather than the charge carriers which are either coupled or decoupled with individual diffusing segments of the matrix. For semicrystalline PEO-based composite electrolytes, T_D corresponds to the onset temperature of the melting peak of the crystalline PEO phase. Such behavior has been previously found for a variety of the composite electrolytes.[35]

Conclusions

It has been shown that the addition of the NNPAAM to polyether-based electrolytes enhances ambient and subambient temperature conductivities by about 1 order of magnitude in comparison to the polyether (OMPEO or PEO)−$LiClO_4$-based system. On the basis of DSC,

FT-IR, and SEM studies, strong interactions are found to occur between the NNPAAM and the dopant salt $LiClO_4$. These interactions in the polyether-NNPAAM−$LiClO_4$ system are of the Lewis acid−base character and lead to the formation of different types of complexes. The formation of type II and III complexes involves the carbonyl oxygen of the NNPAAM molecules and reduces the transient cross-link density in the polyether−$LiClO_4$ system. This leads to the formation of a highly conductive phase, the reason for the observed increase in conductivity. It has been demonstrated that the donicity of the Lewis base centers in NNPAAM is comparable to or even higher than that for the Lewis base oxygens in the polyether. For low concentrations of NNPAAM, this leads to a lowering of the degree of crystallinity of the semicrystalline PEO-based electrolytes. For high NNPAAM concentrations, most of the Li^+ cations are found to be in the NNPAAM phase leaving the polyether phase unaffected and freeing the polyether phase to crystallize. A reduction in the conductivity in this NNPAAM concentration range results. The temperature and concentration dependencies of the conductivity of composite polymeric electrolytes can be described by an EMT approach which qualitatively predicts the conductivity behavior. It has been shown that for OMPEO−NNPAAM−$LiClO_4$ composite electrolytes an increase in the conductivity in comparison to the OMPEO−$LiClO_4$ electrolyte is seen particularly in the subambient temperature region. In this temperature range a deviation from the VTF form is observed. On the basis of the semiempirical model, the crossover temperature T_D ($=T_C$) is measured to be 1.2 times the T_g of the OMPEO−$LiClO_4$ electrolyte which is in agreement with the mode-coupling theory predictions of a change in the diffussion mechanism in this temperature range.

Acknowledgment. Appreciation is expressed to Dr. K. Such who synthesized the OMPEO. W.W. wishes to thank NSERC Canada and the Research Office of NATO for an International Fellowship award. A.Z. wishes to thank the Research Office of NATO for a scholarship according to the NATO linkage grant.

References and Notes

(1) See, for instance: *Polymer Electrolyte Reviews*-1 and *Polymer Electrolyte Reviews-2*; MacCallum, J. R., Vincent, C. A., Eds; Elsevier: London, 1987, 1989.
(2) Gray, F. M. *Solid Polymer Electrolytes-Fundamentals and Technological Applications*; VCH: Weinheim, Germany, 1991.
(3) Scrosati, B. *Applications of Electroactive Polymers*; Chapman and Hall: London, 1993.
(4) Ratner, M. In *Polymer Electrolyte Reviews*-1; MacCallum, J. R., Vincent, C. A., Eds.; Elsevier: London, 1987; Chapter 7.
(5) Berthier, C.; Gorecki, W.; Minier, M.; Armand, M. B.; Chabagno, J. M.; Rigaud, P. *Solid State Ionics* **1983**, *11*, 91.
(6) He, Y.; Chen, Z.; Zhang, Z.; Wang, C.; Chen, L. *Gaodeng Xuexiao Huaxue Xuebao* **1986**, *2*, 97.
(7) Capuano, F.; Croce, F.; Scrosati, B. *J. Electrochem. Soc.* **1991**, *138*, 1918.
(8) Wieczorek, W.; Such, K.; Płocharski, J.; Przyłuski, J. *Proceedings of the II International Symposium on Polymeric Electrolytes, Siena 1989*; Scrosati, B., Ed.; Elsevier Applied Science: London, 1990; p 339.
(9) Wieczorek, W.; Such, K.; Florjańczyk, Z.; Stevens, J. R. *J. Phys. Chem.* **1994**, *98*, 6840.
(10) Wieczorek, W.; Such, K.; Chung, S. H.; Stevens, J. R. *J. Phys. Chem.* **1994**, *98*, 9047.
(11) Wieczorek, W.; Florjańczyk, Z.; Stevens, J. R. *Electrochim. Acta* **1995**, *40*, 2251.
(12) Wieczorek, W.; Such, K.; Florjańczyk, Z.; Stevens, J. R. *Electrochim. Acta* **1995**, *40*, 2417.
(13) Gutmann, V. *Coordination chemistry in nonaqueous solutions*; Springer Verlag: Berlin, 1968; Chapter 2.
(14) Jensen, W. B. *The Lewis acid-base concepts*; Wiley and Sons: New York 1980; Chapter 7.
(15) Nicholas, C. V.; Wilson, D. J.; Booth, C.; Giles, J. R. M. *Br. Polym. J.* **1988**, *20*, 289.
(16) Li, X.; Hsu, S. L. *J. Polym. Sci., Polym. Phys. Ed.* **1984**, *22*, 1331.
(17) Salomon, M.; Xu, M.; Eyring, E. M.; Petrucci, S. *J. Phys. Chem.* **1994**, *98*, 8234.
(18) Schantz, S.; Torell, L. M.; Stevens, J. R. *J. Chem. Phys.* **1991**, *94*, 6862.
(19) Shriver, D. F.; Bruce, P. G. In *Solid State Electrochemistry*; Bruce, P. G., Ed.; Cambridge University Press: Cambridge, 1995; Chapter 5.
(20) Olender, R.; Nitzan, A. *J. Chem. Phys.* **1995**, *102*, 7180.
(21) Latham, R. J.; Linford, R. G. I-st Electronic Conference on Solid State Ionics, June 1995; Paper 314.
(22) Molnar, A.; Eisenberg, A. *Macromolecules* **1992**, *25*, 5774.
(23) Lu, X.; Weiss, R. A. *Macromolecules* **1991**, *24*, 4381.
(24) Li, J.; Khan, I. M. *Macromolecules* **1993**, *26*, 4544.
(25) Gotze, W.; Sjorgen, L. *Rep. Prog. Phys.* **1992**, *55*, 241.
(26) Chung, S. H.; Wieczorek, W.; Such, K.; Stevens, J. R. Manuscript in preparation.
(27) Chung, S. H. Ph.D. Thesis, University of Guelph, Guelph, Ontario, Canada, 1995.
(28) Nan, C. W.; Smith, D. M.; *Mater. Sci. Eng., B* **1991**, *10*, 99.
(29) Nan, C. W. *Prog. Mater. Sci.* **1993**, *37*, 1.
(30) Wieczorek, W.; Siekierski, M. *J. Appl. Phys.* **1994**, *76* (4), 2220.
(31) Nakamura, M. *Phys. Rev. B* **1984**, *29*, 3691.
(32) Kirkpatrick, S. *Rev. Mod. Phys.* **1973**, *45*, 574.
(33) Dienes, G. J. *J. Appl. Phys.* **1950**, *21*, 1189.
(34) Almond, D. P.; West A. R. *Solid State Ionics* **1986**, *18* and *19*, 1105.
(35) Wieczorek, W. *Solid State Ionics* **1992**, *53−56*, 1064.

MA950672N